Chapter 2
Simulation Methods of Quantum-Dot Semiconductor Optical Amplifiers

2.1 Introduction

In modeling a semiconductor optical amplifier, one would first consider how the carrier dynamics are modeled. Secondly, one would be concerned about how to model the optical field propagation. There exist many SOA models of different accuracies. The most accurate way of modeling an SOA is to solve the semiconductor bloch equation (SBE) but this is extremely time-consuming. The computation time is not acceptable for the system applications of SOA-based devices, where many optical pulses have to be transmitted through the SOA to evaluate the system performance. A simplified approach is to include certain physical processes phenomenologically, as it is done in rate-equation models. These models enjoy the much faster calculation speeds. Although the accuracy for sub-picosecond pulses is not as good as the SBE calculations, the rate equation models are quite successful in explaining the experimental results for both laser diodes and SOAs. In early 1990s, Mørk et al. introduced the concept of the local carrier density in the SOA modeling and by doing so, intra-band carrier dynamics such as spectral hole burning, carrier heating and free carrier absorption can be modeled with great success to explain the pump-probe experimental results.

Numerical modeling is always necessary to understand the working principle of the devices and to optimize their performance. It is also useful to verify a novel idea before implementing it in the lab. It also allows the applications engineer to predict how an SOA or cascade of SOAs behaves in a particular application. It means, physical modeling of complex devices including SOA, such as all-active MZIs, is necessary in order to understand their potential and limitations. In addition, a reliable physical model may be used to investigate new configurations leading to superior ways of operating devices, or possibly to development of entirely new device structures.

The main purpose of modeling a SOA is to relate the internal variables of the amplifier to measurable external variables such as the output signal power,

A. Rostami et al., *Nanostructure Semiconductor Optical Amplifiers*,
Engineering Materials, DOI: 10.1007/978-3-642-14925-2_2,

saturation output power and amplified spontaneous emission (ASE) spectrum. This aids the design and optimization of SOA for a given application. As the SOA model equations contain coupled derivatives of time and space, thus they have rarely analytical solutions. However, analytical solutions of SOA equations can give a deep understanding on how internal variables of the device vary by external conditions such as injection current, input pump, temperature, etc. Also, an analytical solution may exactly exhibit the limitation of the operation since it contains the influence of physical phenomena explicitly. Due to the mentioned difficulties of obtaining an analytical solution, a numerical solution is required in most of applications.

Numerical techniques are usually more complex but make fewer assumptions and are often applicable over a wide range of operating regimes. With the advent of fast personal computers, numerical techniques are beginning to supersede analytical techniques.

In spite of intensive research on numerical modeling of QD-SOAs, both theoretically and experimentally, there still remains an unexplored area. This involves the development of equivalent circuit models for QD-SOAs suitable for circuit simulation by using standard packages like SPICE. Considering the fact that numerical techniques as the solution of the rate equations require long and tedious computational time, analysis of equivalent circuit models with circuit programs reduces the computational time several orders.

In this chapter, we bring examples of modeling QD-SOAs by well-known numerical, analytical and equivalent circuits.

2.2 Numerical Methods

A comprehensive model should include the effect of several factors on QD-SOA performance. Most of modeling methods consider quantum dots grown by the Stranski–Krastanov mode as active region for QD-SOAs and thus some presumptions are considered. In this manner, performance of QD-SOAs is primarily dominated by the dynamics of carriers and photons, like carrier relaxation, capture, re-excitation rate into quantum dots, radiative and non-radiative recombination rates of carriers, inhomogeneous broadening of dot resonant energy due to size fluctuation of dots, homogeneous broadening of optical gain due to polarization dephasing rate, coulomb effects between electrons and holes and optical nonlinearities.

The most popular and useful way to deal with carrier and photon dynamics in opto-electronic devices is to solve rate equations for carriers and photons. In the modeling process described in this section, quantum dots are considered to be spatially isolated and each quantum dot exchange carries with the wetting layer. Quantum dots are grouped by their resonant energy so that the model can justify the inhomogeneously broadened gain spectra due to dot size fluctuation and the homogeneous broadening of dots which originates from carrier-LO phonon and carrier-carrier scatterings, has inserted into the rate equations. The homogeneous

broadening plays a crucial rule in processing applications and determines the channel spacing in multi-wavelength operations [1]. Also, an interesting phenomenon happens in quantum dot lasers due to homogeneous broadening where homogeneous broadening of optical gain connects spatially isolated and energetically different quantum dots by bringing the carriers into the central lasing mode by stimulated emission and thus lasing emission with a narrower linewidth takes place even compared with negligible homogeneous broadening case [2].

The schematic of inhomogeneously broadened quantum dot ensemble grouped by the resonant energy of dots and the related photon distribution is illustrated in Fig. 2.1.

Different approaches have been introduced to treat electron and hole dynamics. In a vastly used model, one may consider an electron and a hole as an exciton and use a common time constant for various processes [2, 3]. Separate consideration of electron and hole dynamics is another approach used in the researches [4].

By separate considering the electron and hole dynamics, one can develop a generalized set of equations to consider the effect of different physical phenomena such as carrier doping [5]. So, this section introduces this approach by considering separate time constant for the processes associated with electrons and holes in a quantum dot structure.

Band diagram of a quantum dot group consisting discrete ground and excited energy levels, continuum like upper state (ensemble of dense energy states in each dot which merge into the two-dimensional energy states of the wetting layer) and quantum well-type wetting layer is displayed in Fig. 2.2 where ground states, excited states and upper states are considered to be two-spin degenerate, fourfold degenerate and many-fold degenerate respectively. Finally, quantum dots and photon modes are divided into M ($j = 1, \ldots, M$) and N ($k = 1, \ldots, N$) groups, respectively.

The linear optical gain of ground or excited state of jth quantum dot group to kth photon mode can be expressed as

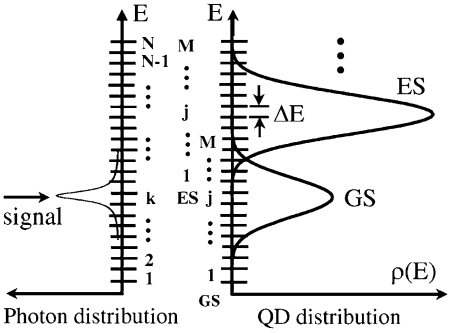

Fig. 2.1 Grouping of inhomogeneously broadened quantum dot ensemble and the related photon mode distribution [5]

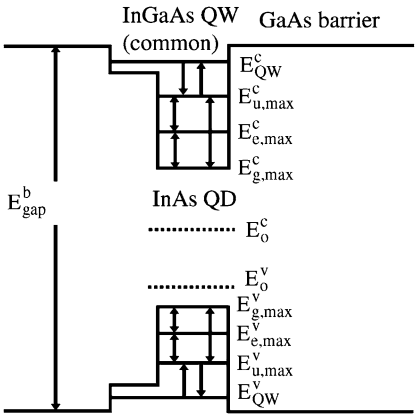

Fig. 2.2 Band diagram of a quantum dot group with maximally allowable energy states defined by $E_{i,max}$ [5]

$$g_{jk}^{g(e)} = \frac{\pi q^2}{n_b c \varepsilon_0 m_0^2 \omega_k} |p_{cv}|^2 D_{g(e)} N_D G_j^s \times \frac{\Gamma_h/(2\pi)}{\left(E^c_{g(e),j} - E^v_{g(e),j} - \hbar\omega_k\right)^2 + (\Gamma_h/2)^2} \tag{1}$$

where p_{cv} is the transition matrix element, c is the velocity of light, q is the electron charge, m_0 is the free electron mass, n_b is the background refractive index, ε_0 is the permittivity of vacuum, N_D is quantum dot volume density, G_j^s is the fraction of the radiative electron–hole recombination from the *j*th quantum dot group which has the Gaussian distribution with the FWHM of $\Gamma_s = \Gamma_c + \Gamma_v = 50$ meV. The degeneracy of ground and excited states denoted by $D_{g(e)}$ are $D_g = 2$ and $D_e = 4$ and their related energy in *j*th group are described by $E^c_{g(e),j}$, for conduction band and $E^v_{g(e),j}$ for valence band. Γ_h is the FWHM of homogeneous broadening ranging from 16 to 19 meV in quantum dot lasers [2] and about 10 meV in quantum dot amplifiers [6]. As it is obvious in (1), a Lorentzian line shape function is used for the homogeneous broadening.

The transition matrix element (neglecting the optical-field polarization dependence) is expressed as

$$|p_{cv}|^2 = |I_{c,v}|^2 \cdot M^2 \tag{2}$$

where $I_{c,v}$ is the overlap integral between the envelope functions of an electron and a hole given by

$$M^2 = \frac{m_0^2}{12 m_e^*} \frac{E_g(E + \Delta)}{E_g + 2\Delta/3} \tag{3}$$

Here, E_g is the band gap, Δ is the spin–orbit splitting energy and m_e^* is the electron effective mass.

The propagation of optical signal and the ASE along the QD-SOA can be expressed by

$$\frac{\partial P(\omega_k, z)}{\partial z} = [\Gamma g(\omega_k, z) - \alpha_i] P(\omega_k, z) \tag{4}$$

$$\frac{\partial P_{sp}(\omega_k, z)}{\partial z} = [\Gamma g(\omega_k, z) - \alpha_i] P_{sp}(\omega_k, z) + \Gamma g_{sp}(\omega_k, z) P_{vac}(\omega_k). \tag{5}$$

P, P_{sp}, α_i, Γ, g_{sp} and P_{vac} are optical signal power, ASE power, intrinsic loss, confinement factor, optical gain for spontaneous emission and the optical power of the vacuum field between the frequency ω_k and $\omega_k + \Delta\omega$ [7].

In self-assembled quantum dots, carriers are injected into the wetting layer and then they are captured by upper states following with relaxation to excited and ground states. Then, the carrier population dynamics of the wetting layer $n_w^{c(v)}$, the upper state $n_{u,j}^{c(v)}$, the excited state $n_{e,j}^{c(v)}$ and the ground state $n_{g,j}^{c(v)}$ of the jth group with corresponding occupation probabilities of $f_w^{c(v)}$, $f_{u,j}^{c(v)}$, $f_{e,j}^{c(v)}$ and $f_{g,j}^{c(v)}$ is described by the following rate equations [5]

$$\begin{aligned} \frac{dn_w^{c(v)}}{dt} &= \frac{J.A}{q} + \sum_j \frac{n_{u,j}^{c(v)}}{\tau_{uw,j}^{c(v)}} \left(1 - f_w^{c(v)}\right) \\ &\quad - \sum_j \frac{n_w^{c(v)}}{\tau_{wu}^{c(v)}} G_j^{c(v)} \left(1 - f_{u,j}^{c(v)}\right) - \frac{\sqrt{n_w^c n_w^v}}{\tau_{wr}} \end{aligned} \tag{6}$$

$$\begin{aligned} \frac{dn_{u,j}^{c(v)}}{dt} &= \frac{n_w^{c(v)}}{\tau_{wu}^{c(v)}} G_j^{c(v)} \left(1 - f_{u,j}^{c(v)}\right) - \frac{n_{u,j}^{c(v)}}{\tau_{uw}^{c(v)}} \left(1 - f_w^{c(v)}\right) \\ &\quad + \frac{n_{e,j}^{c(v)}}{\tau_{eu}^{c(v)}} \left(1 - f_{u,j}^{c(v)}\right) - \frac{n_{u,j}^{c(v)}}{\tau_{ue}^{c(v)}} \left(1 - f_{e,j}^{c(v)}\right) + \frac{n_{g,j}^{c(v)}}{\tau_{gu}^{c(v)}} \left(1 - f_{u,j}^{c(v)}\right) \\ &\quad - \frac{n_{u,j}^{c(v)}}{\tau_{ug}^{c(v)}} \left(1 - f_{g,j}^{c(v)}\right) - \frac{\sqrt{n_{u,j}^c n_{u,j}^v}}{\tau_{dr}} \end{aligned} \tag{7}$$

$$\begin{aligned} \frac{dn_{e,j}^{c(v)}}{dt} &= \frac{n_{u,j}^{c(v)}}{\tau_{ue}^{c(v)}} \left(1 - f_{e,j}^{c(v)}\right) - \frac{n_{e,j}^{c(v)}}{\tau_{eu}^{c(v)}} \left(1 - f_{u,j}^{c(v)}\right) \\ &\quad + \frac{n_{g,j}^{c(v)}}{\tau_{ge}^{c(v)}} \left(1 - f_{e,j}^{c(v)}\right) - \frac{n_{e,j}^{c(v)}}{\tau_{eg}^{c(v)}} \left(1 - f_{g,j}^{c(v)}\right) \\ &\quad - \frac{\sqrt{n_{e,j}^c n_{e,j}^v}}{\tau_{dr}} - \Gamma L \sum_k g_{jk}^e \frac{P_k}{\hbar \omega_k} \left(f_{e,j}^c + f_{e,j}^v - 1\right) \end{aligned} \tag{8}$$

$$\begin{aligned}\frac{dn_{g,j}^{c(v)}}{dt} &= \frac{n_{u,j}^{c(v)}}{\tau_{ug}^{c(v)}}\left(1-f_{g,j}^{c(v)}\right)-\frac{n_{g,j}^{c(v)}}{\tau_{gu}^{c(v)}}\left(1-f_{u,j}^{c(v)}\right)\\ &+\frac{n_{e,j}^{c(v)}}{\tau_{eg}^{c(v)}}\left(1-f_{g,j}^{c(v)}\right)-\frac{n_{g,j}^{c(v)}}{\tau_{ge}^{c(v)}}\left(1-f_{e,j}^{c(v)}\right)\\ &-\frac{\sqrt{n_{g,j}^{c}n_{g,j}^{v}}}{\tau_{dr}}-\Gamma L\sum_{k}g_{jk}^{g}\frac{P_k}{\hbar\omega_k}\left(f_{g,j}^{c}+f_{g,j}^{v}-1\right).\end{aligned} \tag{9}$$

In above equations, J is the input injection current density and A is the cross section area. The transition time constants for carriers are denoted by $\tau_{xy}^{c(v)}$ where the superscript $c(v)$ stands for electron (hole) band and the subscript xy stands for transition from state x to state y $\tau_{eg}^{c(v)}$ determines the relaxation time from the excited state to the ground state for instant). τ_{dr} and τ_{wr} are the recombination time constants in dot and wetting layer, respectively. Typical value of parameters and time constants used in the rate equations can be summarized as, $\tau_{wr} = 0.2$ ns, $\tau_{dr} = 1$ ns, $\tau_{wu}^{c} = 3$ ps, $\tau_{ue}^{c} = \tau_{ug}^{c} = \tau_{eg}^{c} = 1$ ps, $\tau_{wu}^{v} = \tau_{ue}^{v} = \tau_{ug}^{v} = \tau_{eg}^{v} = 0.13$ ps, $D_g = 2$, $D_e = 4$, $D_u^{c(v)} = 10(20)$, $D_w^{c(v)} = 100(200)$, $\alpha_i = 5$ cm^{-1} and $\Gamma = 0.025$.

The value of time constants have obtained from the pump-probe experiments [8], [9] and carrier escape times can be evaluated from the reported relaxation time constants through the relation

$$\tau_{yx}^{c(v)} = \tau_{xy}^{c(v)}\frac{D_y}{D_x}\exp\left(\frac{\Delta E_{xy}^{c(v)}}{kT}\right) \tag{10}$$

where $\Delta E_{xy}^{c(v)}$ is the energy difference between the state y and the state x in the conduction (valence) band.

2.3 Equivalent Circuit Methods

In order to derive an equivalent circuit model of a QD-SOA one should first determine band structure of the active region and then the governing rate equation of the active region should be obtained.

It is assumed that the QDs and WL are surrounded by a barrier material which separates the QD layers to the extent that the dot layers do not couple directly. Furthermore, tunneling between dots within the same layer is neglected. The transition of conduction band ground state (CBGS) to valence band ground state (VBGS) is assumed to be the main stimulated transition by input signal.

Band energy diagram of a quantum dot with related energy levels and intraband relaxation processes considered for extraction of rate equations and subsequent circuit model is illustrated in Fig. 2.3. Here, the rate equations of the active region model are written. The photon propagation equation of input signal and the

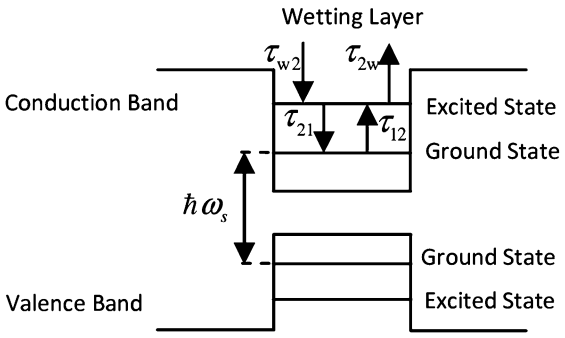

Fig. 2.3 Band energy diagram of a quantum dot with related energy levels and intraband relaxation processes [10]

population dynamics of the wetting layer, the excited state and the ground state can be written as [10]

$$\frac{\partial P_s(z,\tau)}{\partial z} = (g - \alpha_{\text{int}})P_s(z,\tau) \tag{11}$$

$$\frac{\partial N_w(z,\tau)}{\partial \tau} = \frac{I}{eV} - \frac{N_w(1-h)}{\tau_{w2}} + \frac{\tilde{N}_Q h}{\tau_{2w}} - \frac{N_w}{\tau_{wR}} \tag{12}$$

$$\frac{\partial \tilde{N}_Q h(z,\tau)}{\partial \tau} = \frac{N_w(1-h)}{\tau_{w2}} - \frac{\tilde{N}_Q h}{\tau_{2w}} - \frac{\tilde{N}_Q h(1-f)}{\tau_{21}} + \frac{\tilde{N}_Q f(1-h)}{\tau_{12}} \tag{13}$$

$$\frac{\partial \tilde{N}_Q f(z,\tau)}{\partial \tau} = \frac{\tilde{N}_Q h(1-f)}{\tau_{21}} - \frac{\tilde{N}_Q f(1-h)}{\tau_{12}} - \frac{\tilde{N}_Q f^2}{\tau_{1R}} - \frac{g}{\sigma\hbar\omega_s}P_s(z,\tau) \tag{14}$$

where P_s, g and α_{int} are the optical power of input signal, the modal gain, the absorption coefficient of material in signal wavelength, respectively and z is the distance in longitudinal direction, i.e. $z = 0$ and $z = L$ stand for input and output facets of the QD-SOA. $\hbar\omega$ is the photon energy. L_w, σ and V are the effective thickness of active layer, cross section of the quantum dots or active layer and total volume of the quantum dots, respectively. N_Q is the surface density of quantum dots where its typical value is $\sim 5\times10^{10}$ cm^{-2} and $\tilde{N}_Q = N_Q/L_w$ is the effective volume density of quantum dots. Due to the larger effective mass of holes compared to electrons and resulting smaller level spacing, holes are expected to relax faster than electrons [11] and hence, electrons are assumed to limit the carrier dynamics.

The pump term in (12) is given as I/eV, with I being the bias current and e the magnitude of the electronic charge. Current is assumed to be injected directly into the wetting layer and transport phenomena, such as drift or diffusion, are not explicitly included in the model. τ_{wR} is attributed to spontaneous recombination time, which contain contributions from nonradiative, radiative, and Auger recombination. τ_{w2} is the effective capture time and carrier capture is mediated by phonon and Auger processes. Phonon and Auger-assisted capture and relaxation can be taken into account phenomenologically through the relation

$\tau_i = 1/(A + CN_w)$, $i = w2, 21$ where $1/A$ is the phonon-assisted capture (relaxation) time and C is the coefficient determining the rate of Auger-assisted capture (relaxation) by scattering with carriers in the wetting layer. τ_{2w} is the characteristic escape time and τ_{21}, τ_{12} are electron relaxation time from the excited state to the ground state and escape time from the ground state to the excited state, respectively and $\tau_{12} = \tau_{21}$ exp $((E_S - E_G)/k_BT)$ where $E_{S,G}$ are the energies of the excited state and ground state. τ_{1R} is spontaneous radiation lifetime in quantum dots.

The gain expression is given by $g = g_{\max}(f_n + f_p - 1)$ where $g_{\max}$ is maximum modal gain [12] and can be defined as $g_{\max} = \Gamma l\tilde{N}_Q a^{-1} \sum_i \sigma_i(\omega_0)$ where Γ is the confinement factor, l is the number of quantum dot layers, a is the mean size of QD and $\sigma_i(\omega_0)$ is the effective cross section of the QDs at the signal frequency. $f_n(f_p)$ is the electron (hole) occupation probability in the GS. The term $(f_n + f_p - 1)$ is the effective population inversion in GSs where the expressions of f_n and f_p are given in [13]. For simplicity, $f_n = f_p = f$ is assumed [14, 15]. Also $h_n(h_p)$ is the electron (hole) occupation probability in the ES ($h_n = h_p = h$ is presumed).

In order to achieve an input/output model of QD-SOA, we integrate the gain over the length of the device [16]. Therefore, the charge carrier density is supposed to be constant over the SOA length, $N_w(z,\tau) = N_w(\tau), \tilde{N}_Q h(z,\tau) = \tilde{N}_Q h(\tau)$ and also$\tilde{N}_Q f(z,\tau) = \tilde{N}_Q f(\tau)$. Integration of the optical output relation reduces the SOA to a lumped element and averages the internal spatial information to single values, $N_w(\tau), \tilde{N}_Q h(\tau)$ and $\tilde{N}_Q f(\tau)$.

To relate the optical outputs at $z = L$ to the inputs at $z = 0$, one may separate variables of the propagation equation (11), integrate and normalize on $[0, z]$, and solve for the optical power at location z in terms of the input power

$$P_s(z,\tau) = P_s(0,\tau)\exp((g - \alpha_{\text{int}})z) \tag{15}$$

the optical output at the end of the device may describe as

$$P_{s\_out}(\tau) = P_{s\_in}(\tau)\exp((g - \alpha_{\text{int}})L) \tag{16}$$

where L is the SOA length and $P_{s\_in}(\tau) = P_s\ (0,\ \tau)$, $P_{s\_out}(\tau) = P_s\ (L,\ \tau)$. Integrating the ground state rate equation (14) on $z \in [0, L]$ and normalizing by $1/L$ yields

$$\frac{d\tilde{N}_Q f(\tau)}{d\tau} = \frac{\tilde{N}_Q h(1-f)}{\tau_{21}} - \frac{\tilde{N}_Q f(1-h)}{\tau_{12}} - \frac{\tilde{N}_Q f^2}{\tau_{1R}} - \frac{g}{\sigma\hbar\omega}\bar{P}_s(\tau) \tag{17}$$

where Leibnitz's rule has been employed to interchange the time derivative and the spatial definite integral in (17) [17]. It is also defined that

$$\bar{P}_s(\tau) \triangleq \frac{1}{L}\int_0^L P_s(z,\tau)\mathrm{d}z \tag{18}$$

and because f is assumed to be spatially invariant

$$\bar{f}(\tau) \triangleq \frac{1}{L}\int_0^L f(\tau)\mathrm{d}z \tag{19}$$

is simply given by $f(\tau)$ and the over script bar has omitted $\bar{f}(\tau) = f(\tau)$. Substituting (15) into (18) gives

$$\bar{P}_s(\tau) = \frac{P_s(0,\tau)[\exp((g-\alpha_{\text{int}})L) - 1]}{(g-\alpha_{\text{int}})L} \tag{20}$$

So, by substituting (20) into the rate equation (17)

$$\begin{aligned}\frac{\mathrm{d}\tilde{N}_Q f(\tau)}{d\tau} = \frac{\tilde{N}_Q h(1-f)}{\tau_{21}} - \frac{\tilde{N}_Q f(1-h)}{\tau_{12}} - \frac{\tilde{N}_Q f^2}{\tau_{1R}} \\ - \frac{gP_{s\_in}(\tau)[\exp((g-\alpha_{\text{int}})L) - 1]}{V\hbar\omega(g-\alpha_{\text{int}})}\end{aligned} \tag{21}$$

It is possible to rewrite the equations (12) and (13) in a similar manner described above.

Simple algebraic manipulation of new rate equations along with (15) yields equivalent circuit equations as

$$I = C_1\frac{\mathrm{d}v_1}{dt} + \frac{v_1}{R_4} - k_1 v_1 v_2 - k_2 v_2 \tag{22}$$

$$k_3 v_1 + k_4 v_3 + k_5 v_2 v_3 = C_2\frac{\mathrm{d}v_2}{dt} + \frac{v_2}{R_5} + k_6 v_1 v_2 \tag{23}$$

$$k_7 v_2 + k_8 v_2 v_3 = C_3\frac{\mathrm{d}v_3}{dt} + \frac{v_3}{R_3} + k_9 v_3^2 + \zeta v_{s\_in}[\exp(\beta(v_3 - v_{trf})) - 1] \tag{24}$$

$$v_{s\_out} = v_{s\_in}\exp(\beta(v_3 - v_{trf})) \tag{25}$$

where the related parameters are listed below [18]

$$\begin{aligned}i_1 = \frac{eVN_w}{\tau_{w2}} = \frac{v_1}{R_1}, i_2 = \frac{eV\tilde{N}_Q h}{\tau_{21}} = \frac{v_2}{R_2}, i_3 = \frac{eV\tilde{N}_Q f}{\tau_{12}} = \frac{v_3}{R_3}, i_4 = \frac{eVN_w}{\tau_{wR}} = \frac{\tau_{w2}}{\tau_{wR}}i_1, i_5 \\ = \frac{eV\tilde{N}_Q h}{\tau_{2w}} = \frac{\tau_{21}}{\tau_{2w}}i_2, i_6 = \frac{eV\tilde{N}_Q f}{\tau_{1R}} = \frac{\tau_{12}}{\tau_{1R}}i_3,\end{aligned}$$

with $R_1 = R_2 = R_3 = 1\Omega$ and $R_4 = R_1/(1+\tau_{w2}/\tau_{wR}), R_5 = R_2/(1+\tau_{21}/\tau_{2w})$, $C_1 = \tau_{w2}/R_1, C_2 = \tau_{21}/R_2, C_3 = \tau_{12}/R_3, k_1 = k_6 = \tau_{21}/eV\tilde{N}_Q R_1 R_2, k_2 = \tau_{21}/\tau_{2w}$ $R_2, k_3 = 1/R_1$, $R_5 = R_2/(1+\tau_{21}/\tau_{2w})$, $C_1 = \tau_{w2}/R_1$, $C_2 = \tau_{21}/R_2, C_3 = \tau_{12}/R_3$, $k_1 = k_6 = \tau_{21}/eV\tilde{N}_Q R_1 R_2$, $k_2 = \tau_{21}/\tau_{2w}R_2, k_3 = 1/R_1, k_4 = 1/R_3, k_5 = (\tau_{12}-\tau_{21})/$ $eV\tilde{N}_Q R_2 R_3$, $k_7 = 1/R_2$, $k_8 = (\tau_{21}-\tau_{12})/eV\tilde{N}_Q R_2 R_3$, $k_9 = \tau_{12}^2/\tau_{1R}eV\tilde{N}_Q R_3^2$, $\zeta = e^2/\tau_p\hbar\omega_s$, $\beta = 2g_{\max}\tau_{12}L/eV\tilde{N}_Q R_3, v_{trf} = eV\tilde{N}_Q R_3/\ 2\tau_{12}$, $v_{s\_out} = \tau_p P_{s\_out}/e$, $v_{s\_in} = \tau_p P_{s\_in}/e$ with $\tau_p = 1.6 \times 10^{-19}$ s.

It is clear from above definitions that v_1, v_2 and v_3 circuit voltages are proportional to N_w, h and f, respectively. Equations 22–25 can be employed to develop the SPICE circuit model of the QD-SOA as shown in Fig. 2.4a–d with $E1 = v_{s\_in} \exp(\beta(v_3 - v_{trf}))$, $G1 = k_1 v_1 v_2$, $G2 = k_2 v_2$, $G3 = k_3 v_1$, $G4 = k_4 v_3$, $G5 = k_5 v_2 v_3$, $G6 = k_6 v_1 v_2$, $G7 = k_7 v_2$, $G8 = k_8 v_2 v_3$, $G9 = k_9 v_3^2$, $G10 = \zeta v_{s\_in}[\exp(\beta(v_3 - v_{trf})) - 1]$.

The resistors R_{is} and R_{os} are arbitrary. Equations 22–24 are employed to construct equivalent circuit models shown in Fig. 2.4b–d. Considering v_1 as the node voltage in Eq. 22, the four right-hand terms of Eq. 22 are proportional to currents of a capacitor, resistor and voltage-dependant current sources (dependant on node voltages v_1 and v_2) with k_1 and k_2 coefficients, respectively and form the circuit model of Fig. 2.4b for instance. Equation 25 is used to form an equivalent sub-circuit model for V_{s_out} (related to the optical output power of QD-SOA) which is drawn in Fig. 2.4a. These four sub-circuits are coupled to each other to determine the gain saturation characteristics, output power, carrier dynamics and chirp of QD-SOA.

The current source I in Fig. 2.4b is proportional to the SOA bias current in (12), G_1 dependant current source is dependent on v_1 and v_2 variables or N_w and h, respectively and is proportional to the $N_w h/\tau_{w2}$ in (12). The dependant current source G_2 is related to v_2 variable which is proportional to $\tilde{N}_Q h/\tau_{2w}$term and C_1 (capacitance) is the coefficient of wetting layer population variation (τ_{w2}/R_1). All of the parameters can be obtained from other rate equations in a similar manner.

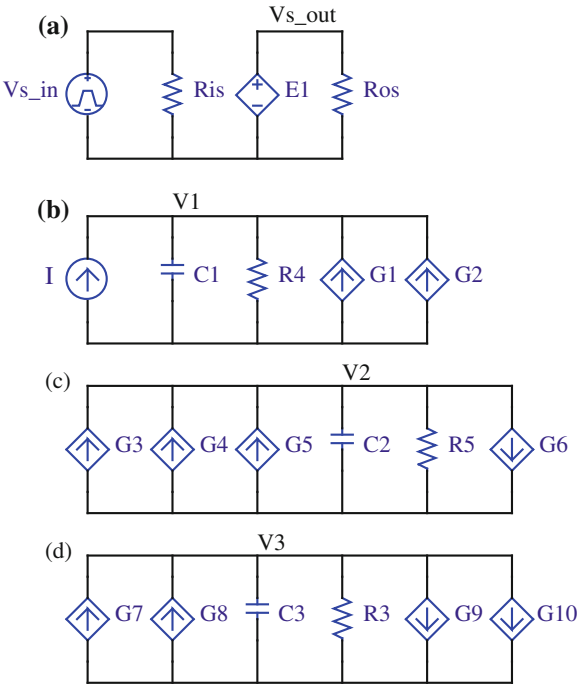

Fig. 2.4 (a) SPICE sub-circuit model to determine the optical output power. (b)–(d) Equivalent sub-circuits to measure V_1, V_2 and V_3, respectively, due to the bias current and V_{s_in} [10]

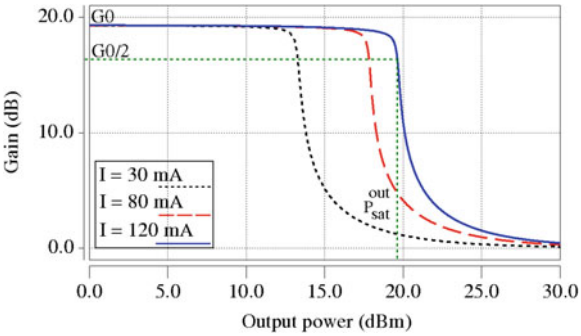

Fig. 2.5 Gain saturation characteristics of a QD-SOA for CW beam amplification, with the SOA gain plotted as a function of the output power, *Pout*, for different pump current *I* in the SOA [10]

To investigate the accuracy of the equivalent circuit model, the gain saturation characteristics, the output pulse shape, the state occupation probabilities and the frequency chirping of the QD-SOA have obtained using SPICE package using the typical parameters given in [19, 20].

The saturation properties with the considered parameters for different bias currents are illustrated in Fig. 2.5. The gain approaches its unsaturated value, G_0, for small optical powers; in present case $G_0 \approx 19$ dB. As the input power (and consequently the output power) is increased, the gain starts to saturate and eventually the amplifier is forced toward transparency.

The output power at which the gain decrease by 3 dB, i.e., at $G_{sat} = G_0/2$ is considered as output saturated power.

Beside the saturation properties, the temporal shape of amplified pulse and the gain dynamic have great importance in QD-SOA operation. As the pulse is amplified inside the SOA, the pulse shape becomes asymmetric due to variation in electronic level population and the leading edge becomes sharper compared with the trailing edge. Sharpening of the leading edge is a common feature of all amplifiers and occurs because the leading edge experiences larger gain than trailing edge [21]. This fact is clear in Fig. 2.6 where the output pulse shape of an input Gaussian pulse is plotted.

Fast gain dynamic is the other issue that should be addressed. The explanation for the fast gain recovery can be seen in Fig. 2.7, which shows the variations of the carrier densities of the three different levels during the amplification of the strong input pulse. As carriers of ground state are removed through stimulated emission the excited state acts as a nearby carrier reservoir and enables ultrafast gain recovery. Since the process of carrier capture is slower than intra-dot relaxation, the excited state recovers on a longer time-scale of several picoseconds which is the upper limit for fast gain recovery time. The long recovery time of the wetting layer is depicted in the inset of Fig. 2.7 which is in several hundred picoseconds timescale.

Since the gain change of SOAs gives rise to changes in the refractive index, a signal that has been amplified or processed with an SOA has a large frequency

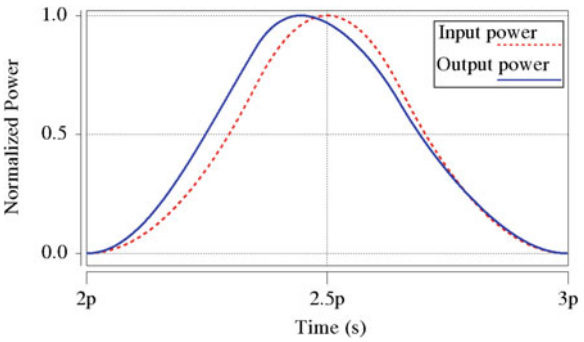

Fig. 2.6 Output pulse shape of a QD-SOA when a Gaussian pulse passes through the amplifier [10]

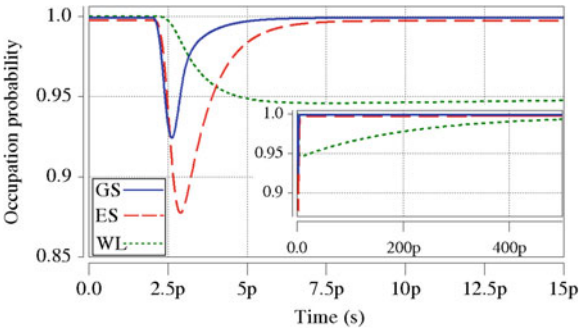

Fig. 2.7 Simulated evolution of occupation probability for the ground state, the excited state and the wetting layer of the QD-SOA. The inset shows the slow dynamics of the wetting layer [10]

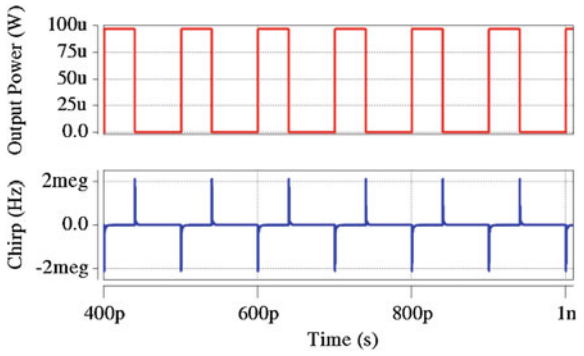

Fig. 2.8 Output power (pulse pattern) and chirp of a pulse train passing through the QD-SOA operating in its linear gain regime, $P_{s\_in} = 10\ \mu W$ [10]

chirp at the leading and trailing edges of the signal pulse. Figures 2.8 and 2.9 show the frequency chirp of the amplified pulses for two input pulse trains at linear ($P_{s\_in} = 10\ \mu W$ (peak value)) and nonlinear ($P_{s\_in} = 10 mW$) operation regions of the QD-SOA. The obtained results for frequency chirp, saturation power and gain recovery process agree well with reported results in mentioned reports (The negligible mismatch is due to $\alpha_{int} = 0$ assumption).

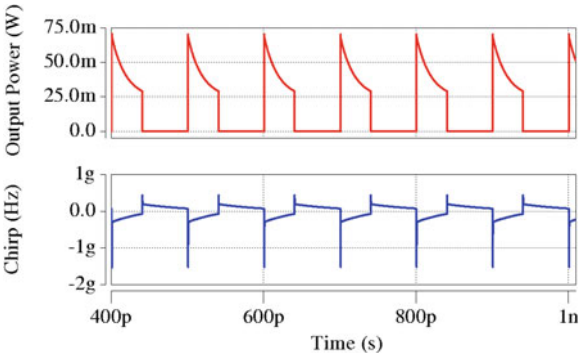

Fig. 2.9 Output power (pulse pattern) and chirp of a pulse train passing through the QD-SOA operating in its nonlinear gain regime, $P_{s\_in} = 10$ mW [10]

2.4 Analytical Methods

Most of the successful models in predicting the optical properties of QD-SOAs treat quantum dots as three-state systems and describe the SOA dynamics based on transitions between the ground state, the excited state and the wetting layer. Therefore, a comprehensive analytical solution for explanation of the operation characteristics of QD-SOAs should take into account the carrier transitions between these three states. The quantum dot model for active region of QD-SOA in this section comprises two nondegenerate energy states (ground and excited states) similar to the model introduced in the previous section. Signal propagation equation through the SOA length and also the rate equations for state occupation probabilities may describe as [22]

$$\frac{\partial S}{\partial z} = [g_{GS}(\hbar\omega)(2f-1) + g_{ES}(\hbar\omega)(2h-1) - \alpha]S \tag{26}$$

$$\frac{\partial f}{\partial t} = \left(\frac{(1-f)h}{\tau_{10}} - \frac{f(1-h)}{\tau_{01}}\right)(a_{10} + c_{10}w) - \frac{f^2}{\tau_{0R}} - \frac{v_g g_{GS}(\hbar\omega)(2f-1)S}{N_Q} \tag{27}$$

$$\frac{\partial h}{\partial t} = \left(\frac{(1-h)w}{\tau_{21}} - \frac{h(1-w)}{\tau_{12}}\right)(a_{21} + c_{21}w) - \left(\frac{(1-f)h}{\tau_{10}} - \frac{f(1-h)}{\tau_{01}}\right)(a_{10} + c_{10}w) - \frac{h^2}{\tau_{1R}} - \frac{v_g g_{ES}(\hbar\omega)(2h-1)S}{N_Q} \tag{28}$$

$$\frac{\partial w}{\partial t} = \frac{J}{\tau_{0R}} - \left(\frac{(1-h)w}{\tau_{21}} - \frac{h(1-w)}{\tau_{12}}\right)(a_{21} + c_{21}w) - \frac{w}{\tau_{wR}}(a_w + b_w w + c_w w^2) \tag{29}$$

The occupation probabilities of the ground state, the excited state and the wetting layer at the band edge are expressed by f, h and w respectively, S is the photon density, α is the waveguide loss, g_{GS} and g_{ES} are the modal gain of the ground and excited states. The phonon-assisted and Auger-assisted processes are included in the rate equations via a_{10}, a_{21}, a_{w} and c_{10}, c_{21}, c_{w} coefficients. Carrier relaxation and excitation processes are denoted by τ_{01}, τ_{10}, τ_{21}, τ_{12}, $\tau_{0\mathrm{R}}$, $\tau_{1\mathrm{R}}$ and τ_{wR} as scape time from the GS to the ES, relaxation time from the ES to the GS, relaxation time from the WL to the ES, escape time from the ES to the WL, spontaneous radiative lifetimes in the GS, ES and WL respectively. N_Q is the quantum dot volume density and J is normalized injection current density ($J = (I \times \tau_{0R})/\, qV_aN_{WL}$ where V_a is the volume and N_{WL} is the carrier density of the WL).

Figure 2.10 describes the variation of the GS occupation probability and photon intensity during SOA length at specified points. When a signal is injected to the SOA at $z = 0$, it experiences unsaturated gain. During the propagation of the signal inside the SOA, the material gain will be decreased and for $z > L_m$ this gain will be equal to material loss. Thus, for $z > L_m$ SOA will be transparent. Meanwhile, the photon intensity increases during the pulse propagation due to stimulated emission and reaches to its maximum value for $z > L_m$.

Therefore, the maximum output density of the devices is expected when the total gain equals with the material loss or $g_{tot} = \alpha$. Since the values of the GS occupation probability and the photon intensity at $z = 0$, z_{ref}, L_m and L will be used to obtain output and threshold characteristics of the SOA, It is useful to define $f\,(z = L_m) = f_m$, $h\,(z = L_m) = h_m$, and $S\,(z = L_m) = S_m$. Considering the photon energy given by $\hbar\omega_0$ and defining $g_{GS}(\hbar\omega_0) = g_0$ and $g_{ES}(\hbar\omega_0) = g_1$ and finding the roots of equation (27) - (29) for $S = 0$, one may obtain the unsaturated occupation probabilities of the GS, ES and WL. It should be noted that this method is valid at steady state and for CW condition where the time derivatives of the carrier rate equations can be set to zero. After evaluating the unsaturated occupation probabilities as f_{us}, h_{us} and W_{us}, the total unsaturated material gain and optical gain of the amplifier may rewrite as

$$g_{tot}^{us} = g_0(2f_{us} - 1) + g_1(2h_{us} - 1) - \alpha \tag{30}$$

$$G_{us} = \exp(g_{tot}^{us} L) \tag{31}$$

and at the $z = L_m$

$$f_m = \frac{1}{2}\left(1 + \frac{\alpha}{g_0}\right) - \frac{g_1(2h_m - 1)}{2g_0}. \tag{32}$$

By replacing the above expression for f_m in (28) and (29), h_m and w_m can be extracted and the maximum output density at $z = L_m$ can be extracted from (27) as (by finding the equivalent value for the expression between parentheses of (29) and replacing in (28) and doing so for (28) and (27)

$$S_m = \frac{g_m}{\alpha} S_{sat} \tag{33}$$

where

$$g_m = g_0\tau_{0R}\left(\frac{J}{\tau_{0R}} - \frac{f_m^2}{\tau_{0R}} - \frac{h_m^2}{\tau_{1R}} - \frac{w_m}{\tau_{wR}}(a_w + b_w w_m + c_w w_m^2)\right) \tag{34}$$

and

$$S_{sat} = \frac{N_Q}{v_g g_0 \tau_{0R}} \tag{35}$$

By introducing the point $z = z_{ref}$ as obvious in Fig. 2.10 with the property $f(z_{ref}) = f_r = (f_{us} + f_m)/2$, the photon density at this point may be evaluated as

$$S_{ref} = \frac{S_{sat}\tau_{0R}}{2f_r - 1}\left(\frac{(1-f_r)h_r}{\tau_{10}} - \frac{f_r(1-h_r)}{\tau_{01}} - \frac{f_r^2}{\tau_{0R}}\right) \tag{36}$$

where h_r can be obtained from f_r similar to h_m and f_m. After a few mathematical manipulation [22] the optical gain of the QD-SOA can be obtained in a closed-form model as

$$\frac{S_{out}}{S_{in}} = e^{g_{tot}^{us}L}\left(\frac{S_m - S_{out}}{S_m - S_{in}}\right)^{\left(1+\frac{S_m}{S_Y}\right)} \approx e^{g_{tot}^{us}L}\left(\frac{S_m - S_{out}}{S_m - S_{in}}\right)^{\left(\frac{S_m}{S_{ref}}-1\right)} \tag{37}$$

where $S_{in} = S(z = 0)$ is the input density, $S_{out} = S(z = L)$ and $S_Y^{-1} = S_X^{-1} - \varepsilon$ with

$$S_X = \frac{S_m}{2(1 - \varepsilon S_m)}\left(\frac{g_0(2f_m - 1) + g_1(2h_m - 1)}{g_0(f_{us} - f_m) + g_1(h_{us} - h_m)}\right) \tag{38}$$

with

$$\varepsilon = \frac{\frac{1}{S_m} - \frac{\rho}{S_{ref}}}{1 - \rho} \tag{39}$$

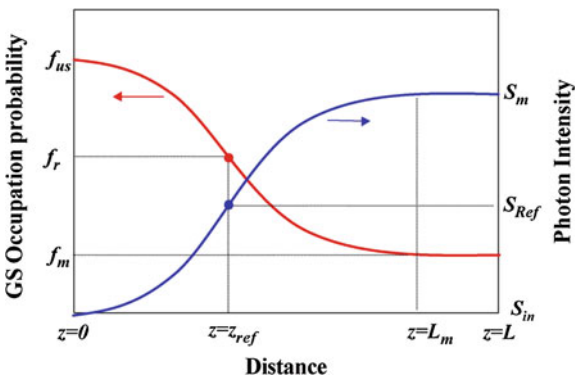

Fig. 2.10 GS occupation probability and photon density at different distances for $S_{in} << S_{sat}$ and $L > L_m$ [22]

and

$$\rho = \frac{[g_0(2f_m - 1) + g_1(2h_m - 1)][g_0(f_{us} - f_r) + g_1(h_{us} - h_r)]}{[g_0(2f_r - 1) + g_1(2h_r - 1)][g_0(f_{us} - f_m) + g_1(h_{us} - h_m)]}. \quad (40)$$

Therefore, the optical gain of the QD-SOA can be obtained analytically only if S_m, S_{ref} and the unsaturated optical gain are known. The output optical gain of the QD-SOA with analytically obtained solution and also with numerical solution of the rate equations using fourth-order Runge–Kutta method have plotted in Fig. 2.11 to compare the accuracy of the solutions.

The following parameters have been used in the simulation; $\tau_{0R} = \tau_{1R} = \tau_{wR} = 0.2$ ns, $\tau_{10} = 8$ ps, $\tau_{21} = 2$ ps, $\tau_{01} = 80$ ps, $\tau_{12} = 20$ ps, $\alpha = 3$ cm^{-1}, $a_{10} = a_{21} = a_w = 1$, $b_w = c_w = 0$, $c_{10} = c_{21} = 80$, $N_Q = 2.5 \times 10^{17}$ cm^3, $v_g = 8.45 \times 10^9$ cm/s, $g_0 = 14$ cm^{-1} and $g_1 = 14$ cm^{-1}. The photon intensity as a function of SOA length is also presented in Fig. 2.12 for both numerical and analytical methods.

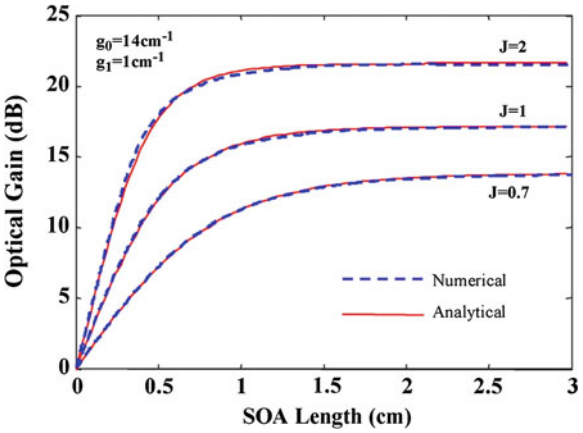

Fig. 2.11 Optical gain of the QD-SOA versus device length for three different applied current values. The Solid lines present the results of analytical method and dashed lines are for numerical method [22]

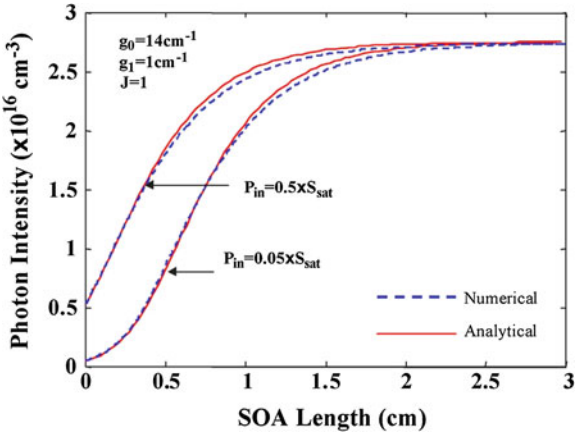

Fig. 2.12 Photon density versus SOA length for two different input signal intensities. The Solid lines present the results of analytical method and dashed lines are for numerical method [22]

By defining the maximum SOA length as the length when the maximum output is 3 dB less than S_m ($S_{out} = 0.5 \times S_m$), one can express an analytical formula for SOA length after which the device provided no gain. Hence, this criteria can be defined from (37) as

$$L < \frac{1}{g_{tot}^{us}} \ln \left(\frac{0.5 S_m}{S_{in}^{\max}} \left[\frac{S_m - S_{in}^{\max}}{S_m - 0.5 S_m} \right]^{\left(1 + \frac{S_m}{S_Y}\right)} \right) \tag{41}$$

As it is obvious from Fig. 2.11, this length is about 1 cm for the given device and for $z > 1$ cm the SOA will be transparent.

References

1. Sugawara, M., Hatori, N., Akiyama, T., Nakata, Y., Ishikawa, H.: Quantum-dot semiconductor optical amplifiers for high bit-rate signal processing over 40 Gbit/s. Jpn. J. Appl. Phys. **40**, L488–L491 (2001)
2. Sugawara, M., Mukai, K., Nakata, Y., Ishikawa, H.: Effect of homogeneous broadening of optical gain on lasing spectra in self-assembled $In_xGa_{1-x}As/GaAs$ quantum dot lasers. Phys. Rev. B **61**, 7595–7603 (2000)
3. Bilenca, A., Eisenstein, G.: On the noise properties of linear and nonlinear quantum-dot semiconductor optical amplifiers: The impact of inhomogeneously broadened gain and fast carrier dynamics. IEEE J. Quantum Electron **40**, 690–702 (2004)
4. van der Poel, M., Gehrig, E., Hess, O., Birkedal, D., Hvam, J.M.: Ultrafast gain dynamics in quantum-dot amplifiers: Theoretical analysis and experimental investigations. IEEE J. Quantum Electron **41**, 1115–1123 (2005)
5. Kim, J., Laemmlin, M., Meuer, C., Bimberg, D., Eisenstein, G.: Theoretical and experimental study of high-speed small-signal cross-gain modulation of quantum-dot semiconductor optical amplifiers. IEEE J. Quantum Electron **45**, 240–248 (2009)
6. Borri, P., Langbein, W., Schneider, S., Woggon, U., Sellin, R.L., Ouyang, D., Bimberg, D.: Exciton relaxation and dephasing in quantum-dot amplifiers from room-to cryogenic temperature. IEEE J. Sel. Topics Quantum Electron **8**, 984–991 (2002)
7. Sugawara, M., Ebe, H., Hatori, N., Ishida, M., Arakawa, Y., Akiyama, T., Otsubo, K., Nakata, Y.: Theory of optical signal amplification and processing by quantum-dot semiconductor optical amplifiers. Phys. Rev. B **69**, 235332-1-39 (2004)
8. Borri, P., Schneider, S., Langbein, W., Bimberg, D.: Ultrafast carrier dynamics in InGaAs quantum dot materials and devices. J. Opt. A **8**, S33–S46 (2006)
9. Dommers, S., Temnov, V.V., Woggon, U., Gomis, J., Martinez-Pastor, J., Laemmlin, M., Bimberg, D.: Complete ground state gain recovery after ultrashort double pulses in quantum dot based semiconductor optical amplifier. Appl. Phys. Lett. **90**, 033508 (2007)
10. Maram, R., Baghban, H., Rasooli, H., Ghorbani, R., Rostami, A.: Equivalent circuit model of quantum dot semiconductor optical amplifiers: dynamic behaviour and saturation properties. J. Opt. A **11**, 105205-1-8 (2009)
11. Sosnowski, T.S., Norris, T.B., Jiang, H., Singh, J., Kamath, K., Bhattacharya, P.: Rapid carrier relaxation in $In_{0.4}Ga_{0.6}As/GaAs$ quantum dots characterized by differential transmission spectroscopy. Phys. Rev. B **57**, R9423–R9426 (1998)
12. Steiner, T. (ed.): Semiconductor Nanostructures for Optoelectronic Applications. Artech House, London (2004)

13. Asryan, L.V., Suris, R.A.: Longitudinal spatial hole burning in a quantum-dot laser. IEEE J. Quantum Electron **36**, 1151–1160 (2000)
14. Qasaimeh, Q.: Characteristics of cross-gain (XG) wavelength conversion in quantum dot semiconductor optical amplifiers. IEEE Photon. Technol. Lett. **16**, 542-544 (2004)
15. Qasaimeh, O.: Optical gain and saturation characteristics of quantum-dot semiconductor optical amplifiers. IEEE J. Quantum Electron. **39**, 793–798 (2003)
16. Saleh, A.A.M.: Nonlinear models of travelling-wave optical amplifiers. Electron Lett. **24**, 835–837 (1988)
17. Kuntze, S.B., Pavel, L., Aitchison, J.S.: Controlling a semiconductor optical amplifier using a state-space model. IEEE J. Quantum Electron **43**, 123–129 (2007)
18. Biswas, A., Basu, P.K.: Equivalent circuit models of quantum cascade lasers for SPICE simulation of steady state and dynamic responses. J. Opt. A **9**, 26–32 (2007)
19. Li X., Li, G.: Comments on "theoretical analysis of gain-recovery time and chirp in QD-SOA". IEEE Photon. Technol. Lett. **18**, 2434–2435 (2006)
20. Ben-Ezra, Y., Haridim, M., Lembrikov, B.I.: Theoretical analysis of gain-recovery time and chirp in QD-SOA. IEEE Photon. Technol. Lett. **17**, 1803–1805 (2005)
21. Agrawal, G.P., Olsson, N.A.: Self-phase modulation and spectral broadening of optical pulses in semiconductor laser amplifiers. IEEE J. Quantum Electron **25**, 2297–2306 (1989)
22. Qasaimeh, O.: Novel closed-form model for multiple-state quantum-dot semiconductor optical amplifiers. IEEE J. Quantum Electron **44**, 652–657 (2008)

http://www.springer.com/978-3-642-14924-5

Nanostructure Semiconductor Optical Amplifiers
Building Blocks for All-Optical Processing
Rostami, A.; Baghban, H.; Maram, R.
2011, IX, 183 p., Hardcover
ISBN: 978-3-642-14924-5